Open pathways for cerebrospinal fluid outflow at the cribriform plate along the olfactory nerves

Irene Spera,[a] Nikola Cousin,[b] Miriam Ries,[b] Anna Kedracka,[b] Alina Castillo,[a] Simone Aleandri,[c] Mykhailo Vladymyrov,[a] Josephine A. Mapunda,[a] Britta Engelhardt,[a] Paola Luciani,[c] Michael Detmar,[b] and Steven T. Proulx[a,*]

[a]Theodor Kocher Institute, University of Bern, Bern, Switzerland
[b]Institute of Pharmaceutical Sciences, ETH Zürich, Zürich, Switzerland
[c]Department of Chemistry, Biochemistry and Pharmaceutical Sciences, University of Bern, Bern, Switzerland

eBioMedicine
2023;91: 104558
Published Online xxx
https://doi.org/10.1016/j.ebiom.2023.104558

Summary

Background Routes along the olfactory nerves crossing the cribriform plate that extend to lymphatic vessels within the nasal cavity have been identified as a critical cerebrospinal fluid (CSF) outflow pathway. However, it is still unclear how the efflux pathways along the nerves connect to lymphatic vessels or if any functional barriers are present at this site. The aim of this study was to anatomically define the connections between the subarachnoid space and the lymphatic system at the cribriform plate in mice.

Methods PEGylated fluorescent microbeads were infused into the CSF space in Prox1-GFP reporter mice and decalcification histology was utilized to investigate the anatomical connections between the subarachnoid space and the lymphatic vessels in the nasal submucosa. A fluorescently-labelled antibody marking vascular endothelium was injected into the cisterna magna to demonstrate the functionality of the lymphatic vessels in the olfactory region. Finally, we performed immunostaining to study the distribution of the arachnoid barrier at the cribriform plate region.

Findings We identified that there are open and direct connections from the subarachnoid space to lymphatic vessels enwrapping the olfactory nerves as they cross the cribriform plate towards the nasal submucosa. Furthermore, lymphatic vessels adjacent to the olfactory bulbs form a continuous network that is functionally connected to lymphatics in the nasal submucosa. Immunostainings revealed a discontinuous distribution of the arachnoid barrier at the olfactory region of the mouse.

Interpretation Our data supports a direct bulk flow mechanism through the cribriform plate allowing CSF drainage into nasal submucosal lymphatics in mice.

Funding This study was supported by the Swiss National Science Foundation (310030_189226), Dementia Research Switzerland—Synapsis Foundation, the Heidi Seiler Stiftung and the Fondation Dr. Corinne Schuler.

Keywords: Cerebrospinal fluid; Lymphatic vessels; Cribriform plate; Olfactory nerves; Arachnoid barrier

Introduction

The anatomical pathways for cerebrospinal fluid (CSF) clearance have not been fully elucidated.[1,2] CSF is predominantly produced by the choroid plexuses within the ventricles and flows unidirectionally into the subarachnoid space (SAS) of the spinal cord and the brain.[3] From the SAS, it was historically considered that the CSF drained mainly into the venous blood via arachnoid granulations or villi extending into the dural venous sinuses.[3–6] However, contrary to this mechanism of drainage into blood, investigators working in a variety of mammalian species found that CSF-injected tracers reached lymphatic vessels, indicating that at least some proportion of CSF drains via the lymphatic system.[7–10] The resultant model of a dual-outflow system (both blood and lymphatic) for CSF has recently been

Abbreviations: CNS, Central nervous system; CSF, Cerebrospinal fluid; E-cadherin, Epithelial cadherin; LP, Lamina propria; ONB, Olfactory nerve bundle; PEG, Polyethylene glycol; Prox1, Prospero homeobox 1; SAS, subarachnoid space; VE-cadherin, Vascular endothelial cadherin

*Corresponding author. Theodor Kocher Institute, University of Bern, CH-3012 Bern, Switzerland.
E-mail address: steven.proulx@tki.unibe.ch (S.T. Proulx).

Research in context

Evidence before this study

Cerebrospinal fluid clearance has been traditionally believed to occur through dural venous sinuses, however, evidence for a route to lymphatic vessels in the nasal cavity has existed for over a century and half. Yet, the anatomical connections at the cribriform plate between the cerebrospinal fluid and the lymphatic system have remained unclear.

Added value of this study

We have performed infusions of fluorescently-labelled micron-sized beads into the cerebrospinal fluid of transgenic lymphatic reporter mice. Using decalcification histology and fluorescent microscopy, we reveal that direct routes exist to the lymphatic vessels in the nasal submucosa for the outflow of cerebrospinal fluid. Lymphatic vessels were found to cross the cribriform plate alongside olfactory nerve bundles to gain access CSF at a location without meningeal barriers.

Implications of all the available evidence

This study has presented the detailed anatomy at a critical link between the central nervous system and the periphery. This drainage route may be important for an immunosurveillance role of the cerebrospinal fluid by providing a route for antigens and cells to reach downstream lymph nodes. Targeting the lymphatics at this location may provide a strategy to improve fluid clearance during brain edema or of proteins involved in neurodegenerative disease.

challenged by in vivo imaging data obtained in mice from our group, showing that the lymphatic system plays the dominant role in CSF clearance.[11–13] However, the anatomical routes from the SAS for CSF to reach the lymphatic system remain unclear.[2]

The CSF-filled SAS is delineated by the arachnoid mater as the outer layer and pia mater as the inner layer. The pia mater consists of a single layer of meningeal cells overlying the glia limitans covering the central nervous system (CNS) parenchyma and is permeable to small solutes.[14,15] The arachnoid mater harbours epithelial-like cells[16] connected by tight junctions[17–19] and adherens junctions.[20] The arachnoid barrier cells form a blood-cerebrospinal fluid barrier (BCSFB) prohibiting free diffusion of water soluble molecules[18,21] and expressing the tight junction protein claudin-11 and the epithelial adherens junction protein E-cadherin.[16,22,23] External to the arachnoid (and thus the CNS proper) is the dura mater, the outermost meningeal layer, which is directly adjoined to the skull or spinal vertebrae. The dura contains an extensive network of blood vessels with properties similar to the periphery, thus allowing the entry of macromolecules and immune cells from the bloodstream into the dural interstitium.[24,25]

While the brain and spinal cord parenchyma are accepted to be devoid of lymphatic vessels, recently lymphatic vessels have been rediscovered in the dura mater.[26,27] Functional tracer data from mice has suggested that the lymphatics located in the dura mater could drain CSF or brain interstitial fluid directly.[26–29] However, at this point, it remains elusive how the CSF and its solutes circumvent the arachnoid barrier to reach this network of lymphatics. Furthermore, data collected from various species over the course of many decades has supported the concept that CSF reaches extracranial lymphatics via routes along cranial nerves and spinal nerves.[2,11,13,30–33] In particular, the route along the olfactory nerves crossing the cribriform plate was deemed especially important.[9,31,34–38]

The axons of olfactory sensory neurons form bundles that travel through foramina in the cribriform plate and synapse on glomeruli in the olfactory bulb.[37] The perineural space alongside the olfactory nerve bundles (ONBs) has been considered by some investigators as a continuation of the SAS, where hydrostatic pressure gradients drive the CSF towards the periphery and into the nasal submucosal lymphatics.[9,35,39] Recent work has identified a network of lymphatics on the CNS side of the cribriform plate which develop postnatally and expand during neuroinflammation.[40–42] However, it still needs to be defined how the lymphatics in the cribriform plate region and nasal submucosal tissue are functionally connected to the SAS and drain CSF to the cervical lymph nodes.[2,43,44] In this context, it is fundamental to investigate the exact anatomical distribution of the arachnoid barrier in respect to the ONBs.

In this study, we have used customized fluorescent microbeads infused in a low volume and at a slow rate into the CSF of transgenic reporter mice to study the outflow pathways at the cribriform plate. We performed decalcification followed by epifluorescence and confocal microscopy to study the anatomical connections from the SAS to lymphatic vessels that drain through the nasal submucosa. Additionally, we aimed to characterize lymphatic vessels within the nasal submucosa and those on the CNS side of the cribriform plate.

Methods

Mice

Male and female Prox1-GFP,[45] Prox1-tdTomato, and Prox1-tdTomato x VE-cadherin-GFP (Mapunda et al., submitted) transgenic reporter mice were bred on the C57BL/6J background to the age of 9–12 weeks. Mice were housed in individually ventilated cages under specific pathogen-free conditions at 22 °C with free access to water and chow.

Ethics

Animal procedures were approved by the Veterinary Office of the Canton Bern (permit no. BE91/19) and have been performed with the recommended protocols for the care and use of laboratory animals in Switzerland and the ARRIVE guidelines.

Formulation of PEGylated microbeads

100 µL of fluorescently-labelled poly(styrene) carboxylate modified beads (PS-COOH) of 1 µm diameter (1% w/w FlashRed; Bangs lab) corresponding to 1 mg of beads (and 43.6 nmol of -COOH group) were washed twice with ultra-purified water (UPW) by centrifugation, then dispersed in 1 mL of anhydrous DMSO (Sigma–Aldrich) and sonicated for 5 min. The mixture was first added with 0.1 mL of 2.2 mg/mL triethylamine (TEA; ACROS organics) solution in DMSO (0.218 mmol) and after a 15 min incubation, 0.1 mL of 1.7 mg/mL (1-[Bis(dimethylamino)methylene]-1H-1,2,3-triazolo[4,5-b]pyridinium 3-oxide hexafluorophosphate) (HATU; Merck) solution in DMSO (0.436 mmol) was also added. The obtained solution was kept under stirring for 15 min and then added to a 2.18 mg (0.436 µmoles) of amine-modified polyethylene methoxy glycol (PEG) with a MW of 5000 Da (MeOH-PEG5K-NH_2). The reaction mixture was sonicated for 3 min and kept at room temperature overnight. The crude was added with 1 mL of UPW and centrifuged (5 min at 15,000 rpm) to remove the DMSO. The particles were collected at the bottom and resuspended in UPW. The washing was performed 4 times to remove also the non-reacted polymer. After the last washing cycle the beads were suspended in 1 mL of PBS 1X and sonicated for 3 min. The hydrodynamic diameter and the polydispersity index (PDI) of the obtained beads were determined by a Litesizer 500 (Anton Paar, Graz, Austria) equipped with a 175° backscatter angle detector and a semiconductor laser with $\lambda = 658$ nm. Briefly, the beads were diluted (1:100) and transferred into disposable semi-micro cuvettes. After equilibrating the sample at 25 °C, the measurement was performed (10 runs × 30 s). The zeta potential was determined by means of continuously monitored phase-analysis light scattering (cmPALS) in an Omega cuvette (Anton Paar, Graz, Austria) where a refractive index of 1.33 and a viscosity of 0.89 mPa/s was set for the solvent. The intensity size distribution of the beads was unimodal; therefore, the autocorrelation function was analysed according to the cumulant method by the Kalliope™-software (Anton Paar). The modified beads had a size of 1306 ± 12 nm, whereas the Zeta potential was –3 mV.

Infusion of microbeads into the lateral ventricle and postmortem in situ imaging

Mice were given a single dose of buprenorphine (Temgesic; 0.375 mg/kg body weight) subcutaneously to provide pain relief and enhance the anaesthesia effect during the surgical procedure. One hour later, mice were anesthetized intraperitoneally (i.p) with a mixture of 80 mg/kg ketamine (Narketan) and 0.4 mg/kg medetomidine (Dormitor) and fixed in a stereotactic frame (RWD, San Diego, CA). A midline skin incision was made to reveal the skull, which was thinned with a dental drill (RWD) at a location 0.95 mm lateral and 0.22 mm caudal to bregma. A 34G Hamilton needle was inserted into the lateral ventricle 2.35 mm ventral to the skull surface. Infusion of 2.5 µL of either unmodified or 0.5% PEG beads at the speed of 1 µL/min was then performed with a syringe pump (Stoelting, Wool Dale, IL). In a subset of experiments, we co-injected 200 µM of P40D800 tracer.[44] The needle was left in place for 2.5 min and then removed slowly while observing if any significant backflow occurred. Mice were sacrificed with an overdose of anaesthesia of ketamine/medetomidine (i.p) at different time points depending on the experiment as detailed in the figure legends. For epifluorescence imaging of the microbeads distribution, a midline incision was made on the front of the neck, and the afferent lymphatics to the superficial cervical lymph nodes were exposed and imaged using a Zeiss AxioZoom.V16 fluorescence microscope (Carl Zeiss, Oberkochen, Germany) equipped with a Plan Neo Fluar Z 1.0×/0.25 objective and CMOS camera (PrimeBSI, Teledyne Photometrics) combined with CoolLED pE-4000 illumination system and GFP and Cy5 filters. Next, the deep cervical lymph nodes were exposed and imaged followed by acquisition of images of the ventral aspect of the skull after removal of the brain. Brains were fixed in 4% paraformaldehyde (PFA) in PBS overnight at 4 °C. Brains were then stored in PBS at 4 °C until sectioning. 100 µm thick sections were obtained using a vibratome (VT1000s, Leica, Wetzlar, Germany). Sections were then mounted on glass slides and left to dry overnight. Images were then acquired using the Zeiss AxioZoom.V16 microscope as described above.

Infusion of tracers into the cisterna magna

Mice were administered buprenorphine analgesia and ketamine/medetomidine anaesthesia as described above. The fur above the dorsal skull and neck of the mice was then shaved. With the help of fine forceps, a dissection microscope and stereotactic frame, an incision above the occipital bone was performed, followed by dissection of the three covering muscle layers. The exposed transparent atlanto-occipital membrane (AOM) then was pierced with a sharpened glass capillary (20–60 µm tip). Then, 5 µL of 0.5 mg/mL anti-mouse CD31-APC (MEC 13.3, BioLegend) or 2.5 µL of 0.5% PEG beads was infused at the speed of 1 µL/min. In addition to the infusion time, the capillary was left 10 min in place to avoid fluid reflux. Before removal of the capillary, a drop of Histoacryl (Braun) was added to the AOM surrounding the capillary. Histoacryl was left to dry shortly to ensure CSF confinement upon capillary

removal. Mice were left in place for an additional 45 min until sacrifice. Mice then were sacrificed followed by decalcification and cryopreservation as described below.

Decalcification histology

For decalcification, mice were transcardially perfused with ice-cold PBS followed by perfusion with 4% PFA in PBS. Mice were then decapitated and the skin, muscles, incisors, and lower jaw were removed from the cranium using forceps and scissors. The whole heads were fixed in 4% PFA overnight and then decalcified in 14% EDTA for 7 days (freshly replaced daily) followed by cryoprotection in 30% sucrose for 3 days. The decalcified heads were embedded in Tissue-Tek OCT Compound, frozen in dry ice and methanol, then stored at –80 °C. Twenty-µm thick frozen sections were obtained using a cryostat (CryoStar NX50, Epredia), mounted on Superfrost plus microscope slides (Epredia, Germany), and stored at –20 °C.

Immunofluorescence staining and imaging

For immunohistochemistry, decalcified frozen sections were thawed at room temperature for 5 min, hydrated with PBS for 10 min, and then permeabilized by 0.1% Triton X-100 (Sigma–Aldrich) in PBS for 10 min. For blocking, 10% donkey serum in PBS was used for 1 h at room temperature. Then, the blocking buffer was removed, and sections were incubated with the blocking buffer of 10% donkey serum containing the primary antibody overnight at 4 °C. This was followed by three washing steps and by incubation with 2% donkey serum in PBS containing the secondary antibody for 2 h at room temperature and protected from light. Before image acquisition, sections were washed three times with PBS and mounted on glass slides with embedding medium Mowiol (Sigma–Aldrich, Steinheim, Germany).

Imaging of decalcified sections was performed with a Zeiss AxioZoom.V16 fluorescence microscope. For Z-stack and higher magnification of sections with microbeads, a Zeiss LSM800 confocal microscope was used. Images were then processed by Fiji software (National Institute of Health, Bethesda, MD).

Antibodies

The primary antibodies used in this study were the following: goat anti-E-cadherin 1:100 dilution (R&D Systems Cat# AF748, RRID: AB_355568), rabbit anti-LYVE-1 1:600 dilution (AngioBio Cat # 11-034, RRID: AB_2813732), goat IgG isotype control antibody 1:100 (R&D Systems Cat# AB-108-C, RRID: AB_354267), and rat anti-LYVE-1 1:200 dilution (ReliaTech Cat# 103-M130). The secondary antibodies used were the following: donkey anti-goat Alexa Fluor 647 1:300 dilution (Jackson ImmunoResearch Cat# 705-605-003, RRID: AB_230436), donkey anti-rabbit Cy3 1:500 dilution (Jackson ImmunoResearch Cat# 711-165-152, RRID: AB_2307443), and donkey anti-rat 488 1:200 (Invitrogen Cat#A21208, RRID: AB_2535794).

Role of funders

The funders had no role in study design, data collection, data analyses, interpretation, or writing of this manuscript.

Results

PEGylated microbeads drain efficiently from the SAS to the lymphatic system

Our group has previously shown that lymphatic vessels are the major outflow pathway for CSF in mice.[11,13,38] Tracers of varying molecular weight have been shown to efflux from the CSF with similar dynamics via routes alongside cranial nerves, implying a bulk outflow process and a lack of tissue barriers.[11] Indeed, previous studies have demonstrated that fluorescent microbeads of up to 1 micron in diameter are found in CNS-draining lymph nodes after injection into the CSF space.[40,42] To study the efflux pathways in greater detail, we first aimed to optimize a formulation of microbeads that would efficiently drain from the CSF to lymphatic vessels and whose distribution would be preserved in relation to anatomical structures on decalcified tissue sections of transgenic lymphatic reporter mice.

Polyethylene glycol (PEG) bound fluorescent tracers appear biologically inert with minimal phagocytosis or retention in tissues, allowing their use as functional tracers for measurements of lymphatic clearance and transport.[46,47] Therefore, we hypothesized that PEGylation of 1 µm diameter microbeads would be advantageous compared to unmodified microbeads to study the CSF outflow pathways through lymphatic vessels. To test this, we developed a protocol to PEGylate microbeads (PEG beads) labelled with the fluorescent dye FlashRed (peak ex: 660 nm; peak em: 690 nm). Then, we infused either unmodified or PEG beads at a volume of 2.5 µL into the right lateral ventricle of Prox1-GFP lymphatic transgenic reporter mice.[45] After 30 min, mice were euthanized and 100 µm brain sections were examined using an epifluorescence microscope (Fig. 1a and b). As shown in Fig. 1a, bright fluorescent signal from the unmodified beads is found on the walls of the ventricles, demonstrating that they are inefficiently cleared and unsuitable for studying CSF flow. On the other hand, minimal signal was detected in the ventricular system after PEG beads infusion, indicating an efficient clearance to the SAS (Fig. 1b). In support of this concept, using fluorescence imaging immediately post-mortem, PEG beads were found along routes leading out of the CNS (Fig. 1c–e). At 30 min after lateral ventricle infusion, after removal of the mouse brain, we observed an accumulation of microbeads at the skull base at the region of the cribriform plate separating the cranial and nasal cavity (Fig. 1c) and

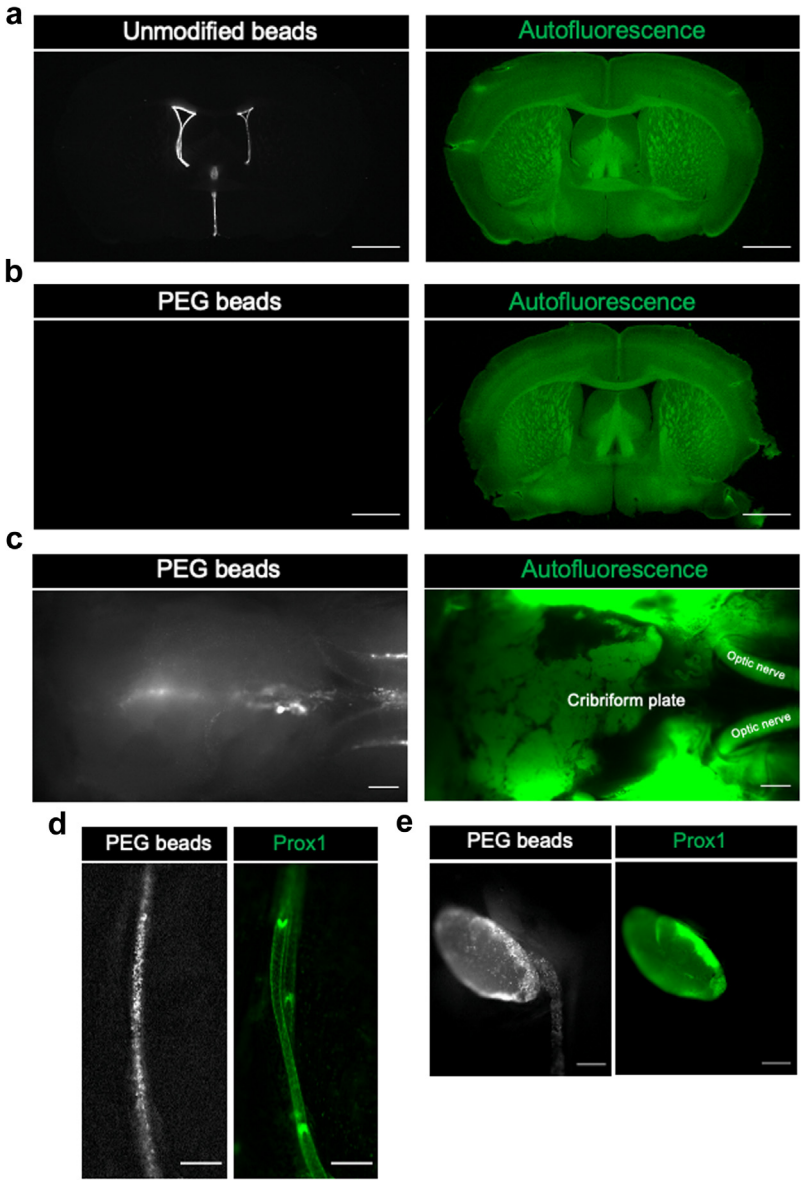

Fig. 1: **PEG beads efficiently clear out of the CNS after lateral ventricular infusion. a** and **b**. Representative images of 100 µm brain sections of a Prox1-GFP reporter mouse 30 min after infusion into the right lateral ventricle of 2.5 µL of unmodified beads (white) (**a**) and PEG beads (**b**). Scale bars: 1 mm. **c–e**. Representative pictures of PEG beads outside the CNS at 30 (**c** and **d**) and 15 min (**e**) after infusion. **c**. PEG beads (white) accumulated at the midline of the cribriform plate at the skull base. Scale bars: 500 µm. **d**. Afferent Prox1^{+} lymphatic vessels (green) leading to the superficial cervical lymph nodes draining PEG beads (white). Scale bars: 200 µm. **e**. PEG beads (white) within the deep cervical lymph nodes and efferent lymphatic vessel (green). Scale bars: 500 µm. **a–e**. Pictures were acquired by an AxioZoom.V16 epifluorescence microscope. Cy5 filter was used to detect the fluorescence of PEG beads (660 nm excitation/690 nm emission). Images are representative of n = 3 mice.

within collecting afferent lymphatics leading to the superficial cervical lymph nodes (Fig. 1d). Already at 15 min after infusion, PEG beads were found draining through the deep cervical lymph nodes to efferent collecting lymphatics (Fig. 1e), showing similar kinetics to our previous studies using 40 kDa PEGylated tracers.[12]

To confirm these findings, we co-injected PEG beads and P40D800 tracer into the lateral ventricle and determined that both clear from the CNS with similar dynamics. Tracer and beads were detected within the deep cervical lymph nodes at 15 min and 30 min after the ventricular infusion. In superficial cervical lymph

nodes, we could confirm that PEG beads and P40D800 tracer were present only at 30 min time point (Supplementary Fig. S1). Thus, these findings suggest a lack of functional barriers between the SAS and the lymphatic system as micron-sized beads rapidly reached the downstream CNS-draining lymphatic vessels.

Nasal submucosal lymphatics drain CSF via direct connections with the SAS

Although the cribriform plate route has been identified in several studies as a crucial CSF outflow pathway, it is still unclear how CSF drains along the olfactory nerves at this location,[2,9,43] with some authors suggesting that CSF must diffuse from the perineural space through the nasal submucosa interstitium to reach the lymphatic vessels.[5,34,35,39,48–50] Therefore, we next aimed to assess the distribution of PEG beads within the nasal cavity after lateral ventricle infusion and a decalcification protocol.[38,41] For this part of the study, we used Prox1-tdTomato transgenic mice to identify lymphatic vessels within the nasal submucosa tissue, which we found to present high autofluorescence at GFP wavelengths. We first assessed if the fluorescent signal of the Prox1-tdTomato reporter mice as well as the anatomical architecture of the nasal submucosa were preserved after the decalcification protocol (Fig. 2a). Indeed, we defined the nasal submucosa consisting of the lamina propria (LP) and the olfactory epithelium (OE) layers, which we found contained Prox1-expressing olfactory sensory neurons. As a connective tissue, the LP harbours blood and lymphatic vessels, mesenchymal cells, ONBs, and the mucus-producing Bowman's glands.[51] Lymphatics expressing the Prox1-tdTomato signal were well-visible in this layer, located typically adjacent to the bony structures of the ethmoid bone, nasal turbinates and septum. DAPI staining allowed us to recognize the morphology of the ONBs embedded in the connective tissue matrix of the LP and the nuclei of the various cell types in the olfactory epithelium. To assess the distribution of PEG beads within the nasal submucosal tissue, we infused microbeads into the right lateral ventricle of Prox1-tdTomato mice, and 20 µm thick decalcified sections were imaged using epifluorescence microscopy.

To gain a general overview at which level along the nasal cavity the PEG beads were distributed, tissue sections were assigned to corresponding transverse regions 1–3 (Fig. 2b), with region 1 close to the nares and region 3 located at the cribriform plate. In region 3 (Fig. 2i–k), where the ONBs cross the cribriform plate, the microbeads were observed mainly in lymphatics in close association with the ONBs or in lymphatic vessels within the LP of the nasal submucosa (Fig. 2j). In region 2 within the nasal tissue (Fig. 2f–h), the microbeads were primarily located in the nasal submucosal lymphatics (Fig. 2g), and some were located in close proximity to the ONBs (Fig. 2g). In region 1 closer to the nares (Fig. 2c–e), there were fewer beads, but they were only found within lymphatics and not surrounding the ONBs (Fig. 2d). In all regions (1–3) of the nasal cavity that we focused on, we could not observe microbeads in the nasal submucosal interstitial tissue (Fig. 2e–k). Moreover, to verify that these findings were not only seen after lateral ventricle infusion, we also performed infusions into the cisterna magna. In this case, we could still observe that the PEG beads were located solely within nasal submucosal lymphatics (Supplementary Fig. S2). Thus, our results indicate that direct connections exist for CSF drainage from spaces around olfactory nerves to lymphatic vessels.

Lymphatic vessels traverse the cribriform plate in close proximity to olfactory nerve bundles and drain CSF-infused microbeads

We next infused Prox1-GFP reporter mice with PEG beads to closely examine the anatomical location and investigate the functionality of the lymphatic vessels at the cribriform plate region. As it is shown in Fig. 3a, we detected a thin network of lymphatic vessels on the CNS side of the cribriform plate extending to the midline between the olfactory bulbs, in agreement with previous studies.[23,40–42]

We examined whether the network of lymphatic vessels found in the nasal submucosa extends through the cribriform plate and is connected to lymphatics on the CNS side.[2,9,36,44] Using confocal microscopy on decalcified coronal sections, we observed that some lymphatics associated with ONBs cross the cribriform plate (Fig. 3a and b) and connect to the network of lymphatics at the midline of the olfactory bulbs (Fig. 3a). Furthermore, these lymphatics appear to completely fill the space between ONBs and blood vessels in the cribriform plate region (Fig. 3b). After infusion into the ventricles, PEG beads were detected both within the lymphatics crossing the cribriform plate (Fig. 3c) and within lymphatic vessels of the nasal submucosal tissue (Fig. 3b and d), indicating that these lymphatics are draining CSF.

These results indicate that part of the network of nasal submucosal lymphatics does not terminate within the submucosal connective tissue. Instead, a portion of these vessels surround ONBs as they cross near the midline of the cribriform plate and appear to function in the drainage of CSF. Therefore, direct routes for CSF outflow are present around ONBs through lymphatic vessels that traverse the cribriform plate.

Lymphatics on the CNS side of the cribriform plate constitute an interconnected network with lymphatics within the nasal cavity

We have recently shown in mice that CSF drainage through the nasal submucosa continues to a network of nasopharyngeal collecting lymphatic vessels leading to the cervical lymph nodes.[38] A recent study has

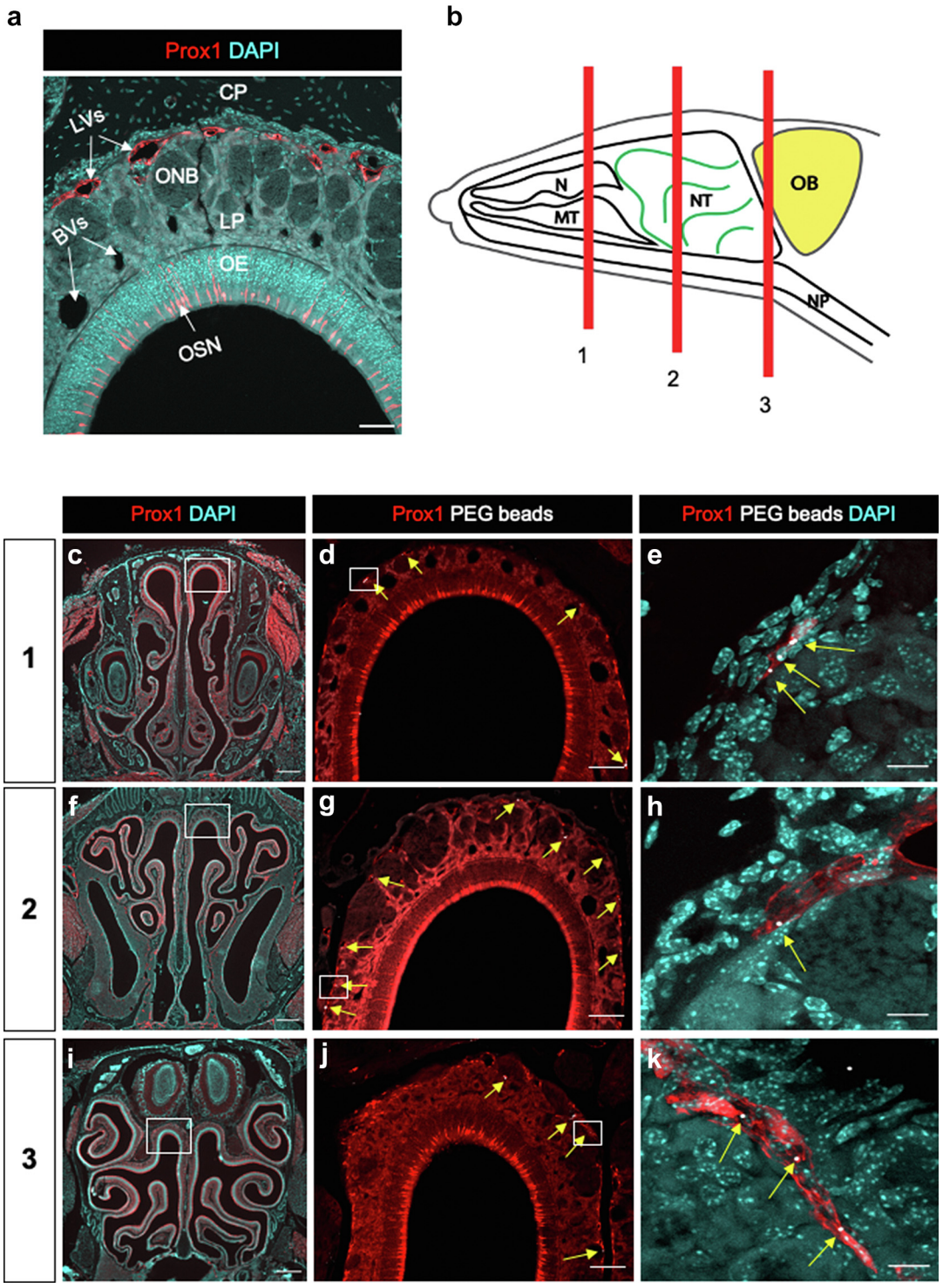

Fig. 2: **Anatomical distribution of PEG beads within the nasal cavity. a**. Decalcified coronal tissue section depicting the nasal submucosa region of a Prox1-tdTomato reporter mouse sacrificed at 45 min after i.c.v infusion. Lymphatic vessels (LVs) in red, olfactory nerve bundles (ONBs), and blood vessels are localized in the lamina propria (LP) layer of the tissue, underneath the cribriform plate (CP). Cell nuclei are shown by DAPI staining (cyan). Olfactory epithelium (OE) harbours cell bodies of Prox1^{+} olfactory sensory neurons (OSNs) in red. Scale bars: 50 µm. Acquired at the confocal microscope. **b**. Schematic of the sagittal plane of the mouse skull and brain showing the regions of interest within the nasal cavity. **c**, **f**, **i**. Representative decalcified coronal sections of the three regions of interest 1–3. Scale bars: 500 µm. **d**, **g**, **j**. Magnification of

demonstrated that the lymphatics in the nasal submucosa lack LYVE-1 expression and may thus represent a separate network of lymphatics from the plexus of lymphatics on the CNS side, which express LYVE-1.[44] However, the existence of Prox1$^+$ lymphatic vessels that cross the cribriform plate appears to challenge this conclusion. Thus, we aimed to further characterize the lymphatics located on the CNS side, within the nasal submucosa, and surrounding the nasopharynx using a panel of lymphatic endothelial markers and injections of labelled antibody.

On coronal sections stained with LYVE-1 antibody, we confirmed that most of the Prox1$^+$ vessels appeared to lack LYVE-1 positivity in the nasal submucosa, while lymphatic vessels on the CNS side of the cribriform plate did indeed stain for LYVE-1 (Fig. 4a and b). LYVE-1 staining was gradually lost in lymphatic endothelial cells as the vessels crossed the cribriform plate but was maintained on a subset of lymphatic endothelial cells on the nasal submucosal side just underneath the cribriform plate (Fig. 4b) and along the septum (Fig. 4c); a portion of the lymphatic vessels around the nasopharynx also showed LYVE-1 positivity (Fig. 4d), while lymphatic vessels surrounding the nasal turbinates did not show evident LYVE-1 signal (Fig. 4e). We detected the same pattern of LYVE-1 immunostaining also on sagittal sections of Prox1-GFP mice (Supplementary Fig. S3a). Although the majority of lymphatics within the nasal submucosa lack LYVE-1 staining, they do appear to be positive for the pan-endothelial marker CD31 and the lymphatic marker podoplanin, as shown on sagittal sections of Prox1-GFP reporter mice (Supplementary Fig. S3b).

Next, we investigated whether there is a functional connection between the lymphatic vessels on the CNS side of the cribriform plate with those within the nasal cavity draining the CSF toward both superficial and deep cervical lymph nodes. Therefore, we injected Prox1-GFP reporter mice with APC-labelled anti-CD31 antibody directly into the CSF at the site of the cisterna magna. The anti-CD31 antibody binds to the CD31 (PECAM-1) receptor expressed on both blood and lymphatic endothelial cells, thus will label invivo any vascular structures that have drained the antibody from the CSF. We allowed the fluorescent antibody to distribute via CSF flow for 30 min prior to sacrificing the mice. Afterwards, sagittal sectioning of decalcified tissue and epifluorescence microscopy were performed to follow the antibody-labelled vessels (Fig. 5a).

Anti-CD31 labelled antibody marked the Prox1$^+$ vessels associated with ONBs crossing the cribriform plate into the nasal submucosa and exposed a continuous network connecting the lymphatics on the CNS side with the lymphatics in the nasal submucosa (Fig. 5b). We followed the vessels into the nasal submucosa where the anti-CD31-labeled antibody colocalized with a rich Prox1$^+$ vascular network (Fig. 5c). The anti-CD31 labelled vessels then converged at the nasopharyngeal area (Fig. 5d) and the vessels continued to be labelled in the region of the nasopharynx (Fig. 5e). Finally, the labelled antibody was detected in both the deep (Supplementary Fig. S4a) and the superficial cervical (Supplementary Fig. S4b) lymph nodes.

As a result of labelled antibody infusion into the CSF, we suggest that nasal lymphatics form a continuous network draining the CSF from the CNS site of the cribriform plate via the nasal submucosa towards the nasopharynx where lymph eventually reaches the draining lymph nodes. Therefore, these findings indicate that nasal submucosal lymphatics are anatomically and functionally connected with the lymphatics present on the CNS side of the cribriform plate.

The arachnoid barrier is discontinuous on the CNS side of the cribriform plate and in the nasal submucosa

Next, we wanted to anatomically delineate the meningeal and perineural layers at the olfactory region to shed more light on how the lymphatic vessels gain access to the SAS to drain the CSF through the cribriform plate. Previous studies have suggested discontinuity of the arachnoid barrier layer above the cribriform plate in rats[52,53] and in mice,[23] possibly indicating that lymphatics can directly access the CSF-draining space.

To study the anatomical structures of the olfactory region, we used Prox1-tdTomato x VE-cadherin-GFP reporter mice, which allowed us to distinguish the lymphatics and the adherens junctions in the blood and lymphatic endothelial cells. We have recently shown that VE-cadherin, beyond its expression on endothelial cell junctions, is also a marker for cells of the pia and arachnoid mater (Mapunda et al., submitted). To specifically identify the arachnoid barrier, we performed immunofluorescence staining on decalcified sections for the epithelial adherens junction protein E-cadherin to detect the epithelial-like cells that compose this barrier.[23,28,54]

the nasal submucosal region showing the distribution of the PEG beads (white) with respect to the LVs in red and the nasal submucosal interstitium. Scale bars 100 µm. **e**, **h**, **k**. Confocal magnified views with maximum intensity projection (MIP) depicting PEG beads (white) within the lumen of the nasal submucosal lymphatics. Scale bars 10 µm. **c–j**. Acquired with an AxioZoom epifluorescence microscope. Images are representative of n = 5 mice. OB = olfactory bulb; CP = cribriform plate; LP = lamina propria; LVs = lymphatic vessels; ONB = olfactory nerve bundle; BVs = blood vessels; OE = olfactory epithelium. Images are representative of n = 4 mice.

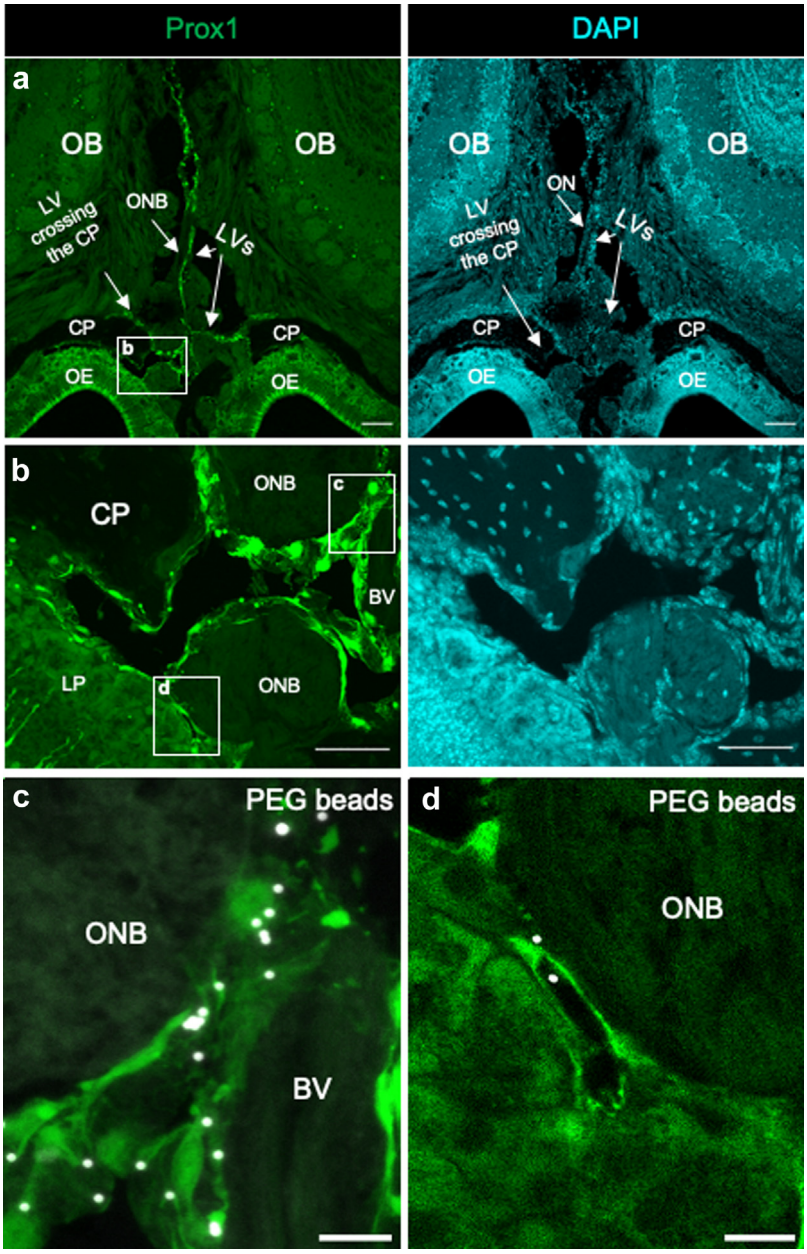

Fig. 3: **Visualization of PEG microbeads within lymphatic vessels crossing the cribriform plate. a**. Coronal overview of a decalcified section at the cribriform plate region of a Prox1-GFP reporter mouse sacrificed at 45 min after i.c.v infusion. Lymphatic vessels (LVs) and olfactory sensory neurons (OSNs) are depicted in green, and cell nuclei (cyan) are shown with DAPI immunofluorescence staining. Scale bars 100 µm. **b**. Magnified view with maximum intensity projection of a lymphatic vessel crossing the cribriform plate and surrounding the olfactory nerve bundle (ONB) and blood vessel (BV). Scale bars: 50 µm. **c** and **d**. PEG beads were detected in the lumen of lymphatics (green) crossing the cribriform plate (**c**) and in those located in the lamina propria of the nasal submucosa (**d**). Scale bars: 10 µm. **a–d**. Acquired with the confocal microscope. Images are representative of n = 3 mice. OB = olfactory bulb; CP = cribriform plate; LP = lamina propria; LV = lymphatic vessel; ONB = olfactory nerve bundle; OE = olfactory epithelium.

We first validated this approach by assessing the meningeal layers of the optic nerve, which is well-described to be ensheathed by both dura and arachnoid mater as outermost layers and by the pia mater as the inner layer. Thus, the arachnoid barrier is considered to be preserved along the optic nerve as it exits the skull.[55] Indeed, we confirmed these previous findings on decalcified sections from the Prox1-tdTomato x

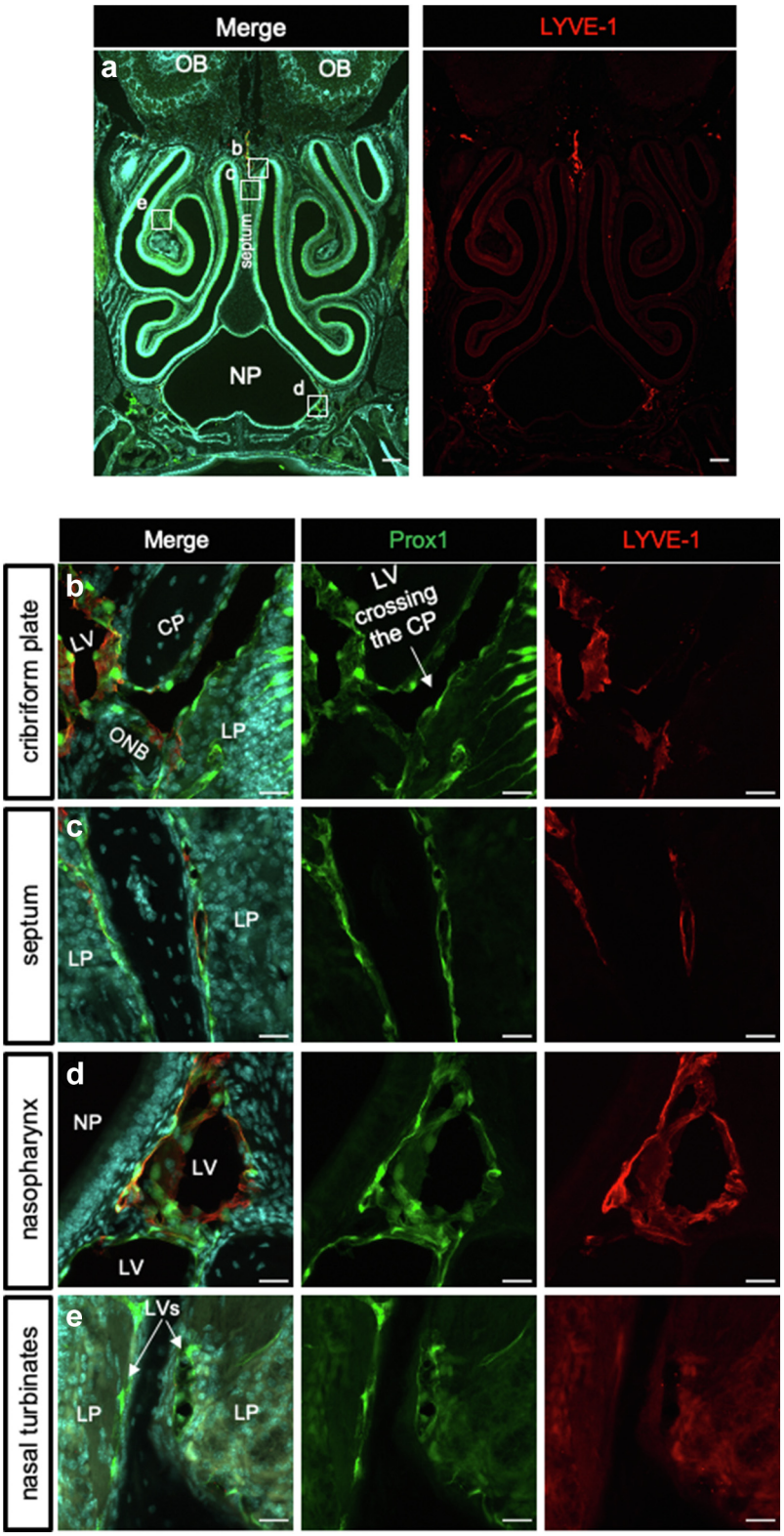

Fig. 4: **Lymphatic vessels crossing the cribriform plate demonstrate a loss of immunostaining for LYVE-1 towards the nasal submucosa.** **a**. Coronal overview of a decalcified section of a Prox1-GFP reporter mouse stained with DAPI (cyan) and LYVE-1 antibody (red). Acquired by the

VE-cadherin-GFP reporter mouse model. VE-cadherin marking the pia and arachnoid mater overlapped partially with the E-cadherin signal (Supplementary Fig. S7), which was intact even outside the skull (Supplementary Fig. S5c).

Next, we assessed the anatomical configuration of the meningeal layers at the olfactory region. We observed that the arachnoid barrier is intact on the dorsal surface of the olfactory bulbs and between the olfactory bulbs (Fig. 6b; Supplementary Fig. S6a). Around the ONBs found on the CNS side of the cribriform plate, discontinuations in the E-cadherin immunostaining were apparent (Fig. 6c; Supplementary Fig. S4a) and a lack of staining was found in the nasal submucosa around the ONBs (Fig. 6c). We also detected the GFP signal for VE-cadherin marking the pia and arachnoid layers between the olfactory bulbs (Fig. 6b; Supplementary Fig. S5a), which partially overlapped with the E-cadherin signal (Supplementary Fig. S7d). Moreover, VE-cadherin bordered the ONBs with a stronger signal on the CNS side of the cribriform plate (Fig. 6c; Supplementary Fig. S5c; Fig. 7b) than in the nasal submucosa (Figs. 6d and 7b).

Notably, we observed that the lymphatic vessels closely surround the ONBs at specific locations where the arachnoid barrier is lacking on the CNS side of the cribriform plate (Fig. 7a) and in the nasal submucosa (Fig. 7b). These findings indicate that mice do not have a classically defined perineural space bordered by continuous pia and arachnoid layers around the ONBs. Instead, we propose a subset of ONBs are surrounded by lymphatic vessels, which serve as conduits for drainage of CSF and macromolecules towards cervical lymph nodes (Fig. 8).

Discussion

In this study, we have anatomically characterized the CSF outflow pathways in the olfactory region of mice by employing CSF infusions of PEG microbeads or labelled antibody into transgenic reporter mice. We first developed a novel formulation of PEGylated microbeads that efficiently cleared from the lateral ventricles to the CNS-draining lymphatic system. Using a decalcification protocol and fluorescence microscopy of tissue sections from lymphatic reporter mice, we localized the beads within nasal submucosal lymphatic vessels and identified beads within the lumen of lymphatic vessels crossing the cribriform plate alongside ONBs. We then demonstrated the existence of a continuous functional network of lymphatic vessels with a unique expression pattern of LYVE-1, draining CSF from the SAS through the nasal submucosa to the collecting vessels around the nasopharynx. Finally, we show that, unlike the situation surrounding the optic nerve, the arachnoid does not form a continuous sheath around ONBs as they exit the skull, thus providing a direct, open route for CSF efflux to perineural lymphatic vessels.

PEGylation is a chemical procedure widely used in drug delivery with the advantage to restrict phagocytosis and limit retention in the tissue after infusion.[56] PEG beads cleared out efficiently from the CNS, reaching the lymphatic system at time points as early as 15 min after infusion into the CSF. The kinetics we observed were similar to smaller tracers used in our previous studies,[12,38] supporting the concept of a bulk flow efflux of CSF to the lymphatic system with open communication between the SAS and the lymphatic vessels. Moreover, the large size of the beads allowed for their identification within lymphatic vessels and draining lymph nodes during post-mortem in situ imaging, as well as on tissue sections after decalcification. While we have confirmed earlier work demonstrating the outflow of microbeads of 0.5–1 μm diameter from the CSF to draining cervical lymph nodes,[40,42] our study has now utilized these tracers to characterize in detail the anatomical connections between the SAS and lymphatics at the cribriform plate.

Several studies have shown that the efflux that occurs through the cribriform plate is an important CSF clearance pathway in mice and other mammalian species.[31,34,36,38,57] However, there is still a lack of consensus on whether CSF drains indirectly to the lymphatic system via diffusion through the interstitial tissue of the submucosa,[5,34,35,39,48–50] or whether there are direct connections between the CSF and the nasal submucosal lymphatics.[36,57,58] In our study, we did not observe diffusion of microbeads within the nasal interstitium in any of the regions of the nasal cavity that we evaluated. Instead, fluorescent imaging revealed that PEG beads could be localized within the lumen of lymphatics of the lamina propria. Thus, direct pathways to lymphatics occur at this level for molecules of at least 1 μm in size. It is essential to highlight that many previous studies investigating the mechanism of CSF outflow pathways at the cribriform plate have used experimental approaches that may not have been ideal for studying CSF bulk outflow. As barriers do not appear to be present around the ONBs after they exit the skull, a diffusion of low molecular weight tracers into the surrounding lamina propria could have occurred in earlier studies, which may have been interpreted as evidence

AxioZoom epifluorescence stereomicroscope. Scale bar: 100 μm. **b–e**. Magnified confocal images depicting lymphatic vessel (green) crossing the CP (**b**), nasal septum (**c**), the area surrounding the nasopharynx (**d**), and lamina propria of nasal turbinates (**e**). Scale bar: 20 μm. Images are representative of n = 3 mice. ONB = olfactory nerve bundle; LV = lymphatic vessel; NP = nasopharynx; LP = lamina propria; CP = cribriform plate.

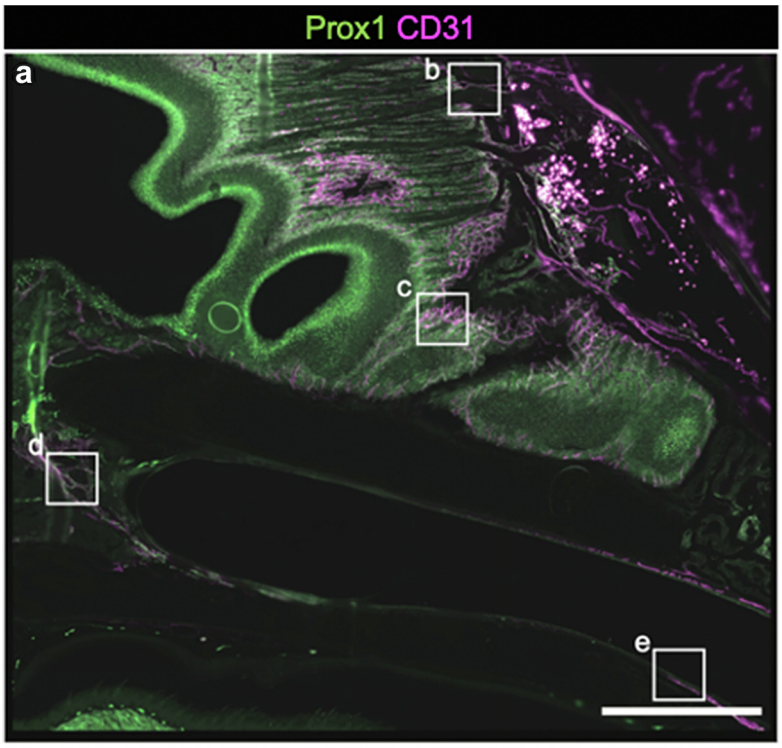
Prox1 CD31
a
b
c
d
e

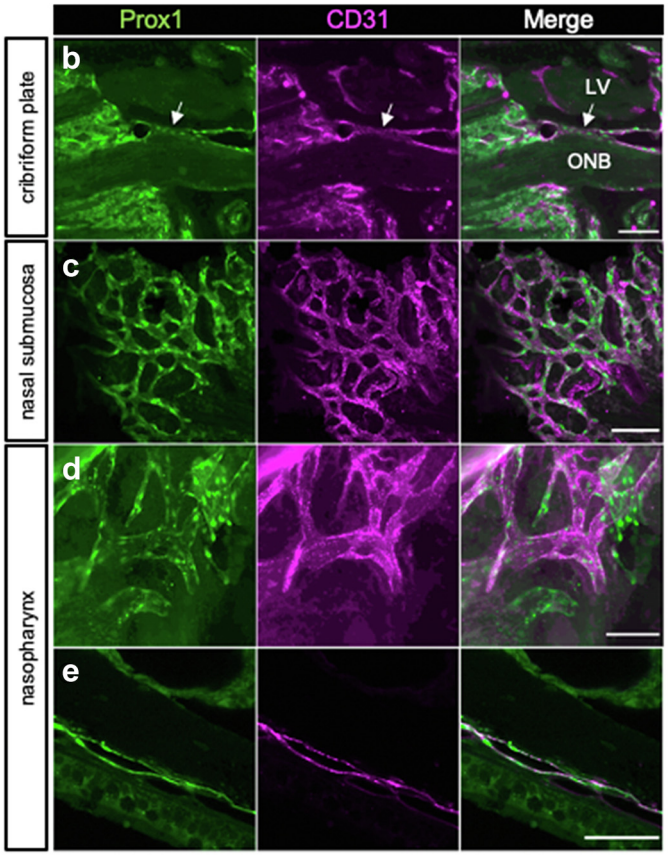
Prox1
CD31
Merge
cribriform plate
nasal submucosa
nasopharynx
b
c
d
e
LV
ONB

for an efflux pathway through the tissue. Other studies have injected tracers post-mortem into the SAS.[57] While in mice a direct uptake of the tracer into the nasal draining lymphatics was observed, on the other hand, the human samples showed limited lymphatic perfusion and a diffusion of the MicroFil into the nasal submucosal interstitium.[57] As the authors acknowledged, the variability of the results might have been affected by abnormal pressures induced by the cadaveric injection and the degradation of the tissue occurring after death.

The literature proposes two different anatomical models for a direct connection between the olfactory perineural space and the nasal submucosal lymphatics. Direct routes could occur via close relationship between the lymphatic vessels and ONBs in the nasal submucosa tissue,[57,58] or, alternatively, lymphatics could cross the cribriform plate to drain CSF.[36,40–42] The data from this study cannot rule out either of these models. In decalcified sections of lymphatic reporter mice, we did indeed observe lymphatics crossing the cribriform plate, maintaining a close connection with the ONBs and reaching the midline between the olfactory bulbs. Moreover, 1 μm beads drained into the lymphatic vessels crossing the cribriform plate on the CNS and the nasal submucosal side. We also observed, similar to previous investigators, that lymphatic vessels appeared to closely surround the olfactory nerves in a "collar-like" fashion.[57,58] We propose that CSF maintains close contact to the ONBs until sites with directly adjacent lymphatic vessels are reached, which may occur on the CNS side of the cribriform plate, while the ONBs are exiting through the bone or within the nasal submucosa. To our knowledge, such an anatomical configuration for direct routes to lymphatic vessels is exclusive to the olfactory region. The closest known anatomical correlate would be the peritoneal or pleural cavities which have been shown to drain fluid through stomata in their mesothelial linings which feed directly into lymphatic vessels. Assuming a steady outflow of CSF occurs through the cribriform plate, direct connections between the CSF and lymphatic draining vessels could be fundamental to protecting the brain from the spread of infectious agents that have infiltrated the extracellular space of the nasal submucosa through the olfactory epithelial layer. In this scenario, bacteria and non-neurotropic viruses would need to spread against the current of the fluid efflux to reach the CNS, potentially limiting their access to the CSF space and instead being routed towards draining lymph nodes.

A recent study has suggested that the lymphatics on the CNS side of the cribriform plate, referred to by these authors as meningeal lymphatics, may represent a separate network from the lymphatic vessels in the nasal submucosa.[44] Using light sheet microscopy of the whole mouse head after CSF injection of fluorescently-labelled ovalbumin tracer and LYVE-1 antibody staining, these authors revealed that lymphatic vessels lack LYVE-1 staining in the nasal submucosa, unlike the meningeal lymphatics on the CNS side of the cribriform plate. In line with their results, we confirmed that lymphatics have a peculiar immunostaining pattern for LYVE-1 in the nasal submucosa. We found Prox1$^+$ lymphatics were positive for LYVE-1 on the CNS side of the cribriform plate and also around the nasopharynx. Such vessels were still LYVE-1$^+$ on the nasal side just underneath the cribriform plate and along the septum, in agreement with a previous study.[59] However, indeed, the submucosa tissue appeared devoid of LYVE-1 signal. Although the LYVE-1 receptor is not an exclusive marker for lymphatic endothelial cells (LECs), it is usually a reliable indicator to distinguish between capillary and collector lymphatics.[60,61] LECs making up blind-ended lymphatic capillaries are connected by discontinuous junctions, express LYVE-1, and lack smooth muscle cells (SMCs) and valves. In contrast, collector lymphatics have continuous cell–cell junctions, SMCs, and intraluminal valves while negative for LYVE-1. Indeed, the rich network of lymphatics in the nasal submucosa that we visualized resembles lymphatic capillaries despite lacking LYVE-1 staining. Furthermore, we observed that labelled CD31 antibody injected into the cisterna magna stained the lumen of LVs crossing the cribriform plate and marked the lymphatics within the nasal cavity at the level of the nasal submucosa and around the nasopharynx. These functional data, in combination with our staining of lymphatic vascular markers podoplanin and CD31 within the lymphatic plexus in the nasal submucosa, suggests that lymphatics on the CNS side of the

Fig. 5: **APC labelled anti-CD31 antibody reveals a continuous CSF outflow pathway through lymphatic vessels at the cribriform plate to nasopharyngeal lymphatics. a**. Representative sagittal view of sectioned Prox1-GFP mouse skull of the nasal cavity 50 min after injection of APC-labelled anti-CD31 antibody into the cisterna magna. Lymphatic vessels are shown in green (Prox1). Labelled antibody in magenta (CD31) was detected at the site of the cribriform plate, throughout the nasal submucosa, and in intravascular spaces in the nasopharyngeal area and the pharynx. Regions of interest **b–e** are marked by boxes. Scale bar: 1 mm. Sagittal regions with Prox1$^+$ (green) and CD31$^+$ (magenta) vessels follow from the cribriform plate via the nasal submucosa down to the nasopharynx. **b**. Antibody deposition in Prox1$^+$ vessels and around olfactory nerves crossing the cribriform plate into the nasal submucosa (indicated by arrows, scale bar: 100 μm). **c**. Labelled antibody exposed a vast Prox1$^+$ lymphatic vascular network stretched over the nasal submucosa (scale bar: 50 μm). **d**. Drainage of the labelled antibody into the nasopharyngeal area (scale bar: 50 μm) and **e**. further down the nasopharynx (scale bar: 100 μm). Images are representative of n = 3 mice. ONB = olfactory nerve bundle; LV = lymphatic vessel.

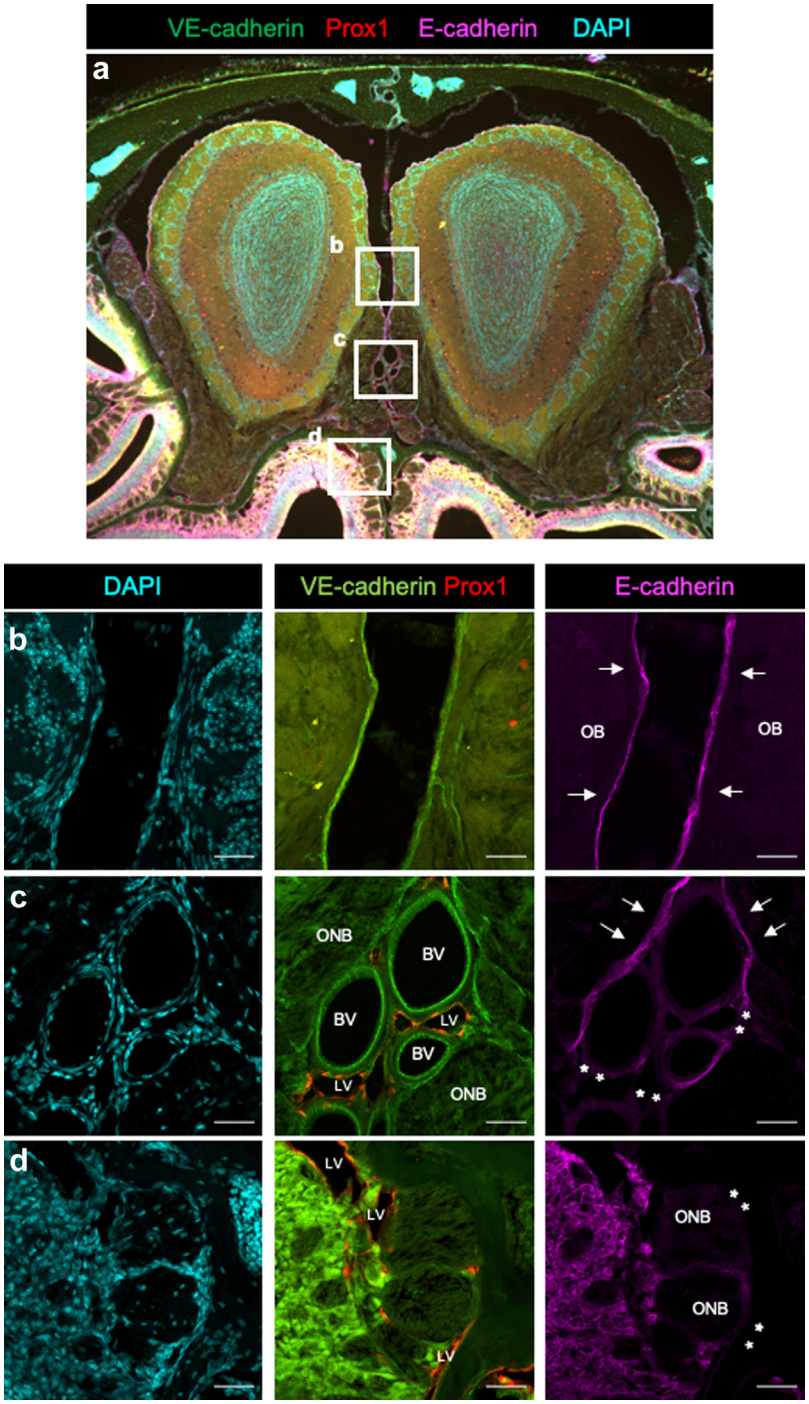

Fig. 6: **The arachnoid is interrupted between olfactory nerve bundles and lymphatic vessels. a**. Representative decalcified coronal overview of the olfactory bulbs, cribriform plate, and nasal submucosa of Prox1-tdTomato x VE-cadherin-GFP transgenic mouse immunolabeled with E-cadherin antibody. Acquired with an AxioZoom epifluorescence microscope. Scale bar: 200 µm. **b–d**. Magnified images of the white insert show the region between the olfactory bulbs (**b**), the CNS side of the cribriform plate (**c**), and the nasal submucosa (**d**). Z-stacks acquired by confocal microscope and Sum Intensity Projection were reconstructed with Fiji software. Cell nuclei are shown with DAPI staining (cyan). VE-cadherin-GFP^{+} cells (green) are detected on the surface of the olfactory bulbs (**b**), on the blood (BV) and lymphatic vessels (LV), and around the olfactory nerve bundles (ONBs) (**c** and **d**). E-cadherin antibody (magenta) was found on the surface of the olfactory bulbs (**b**), interrupted on the CNS of the cribriform plate (**c**), and in the nasal submucosa (**d**). Scale bar: 20 µm. White asterisks indicate discontinuity of the arachnoid barrier; white arrows show the arachnoid mater intact. Images are representative of n = 5 mice.

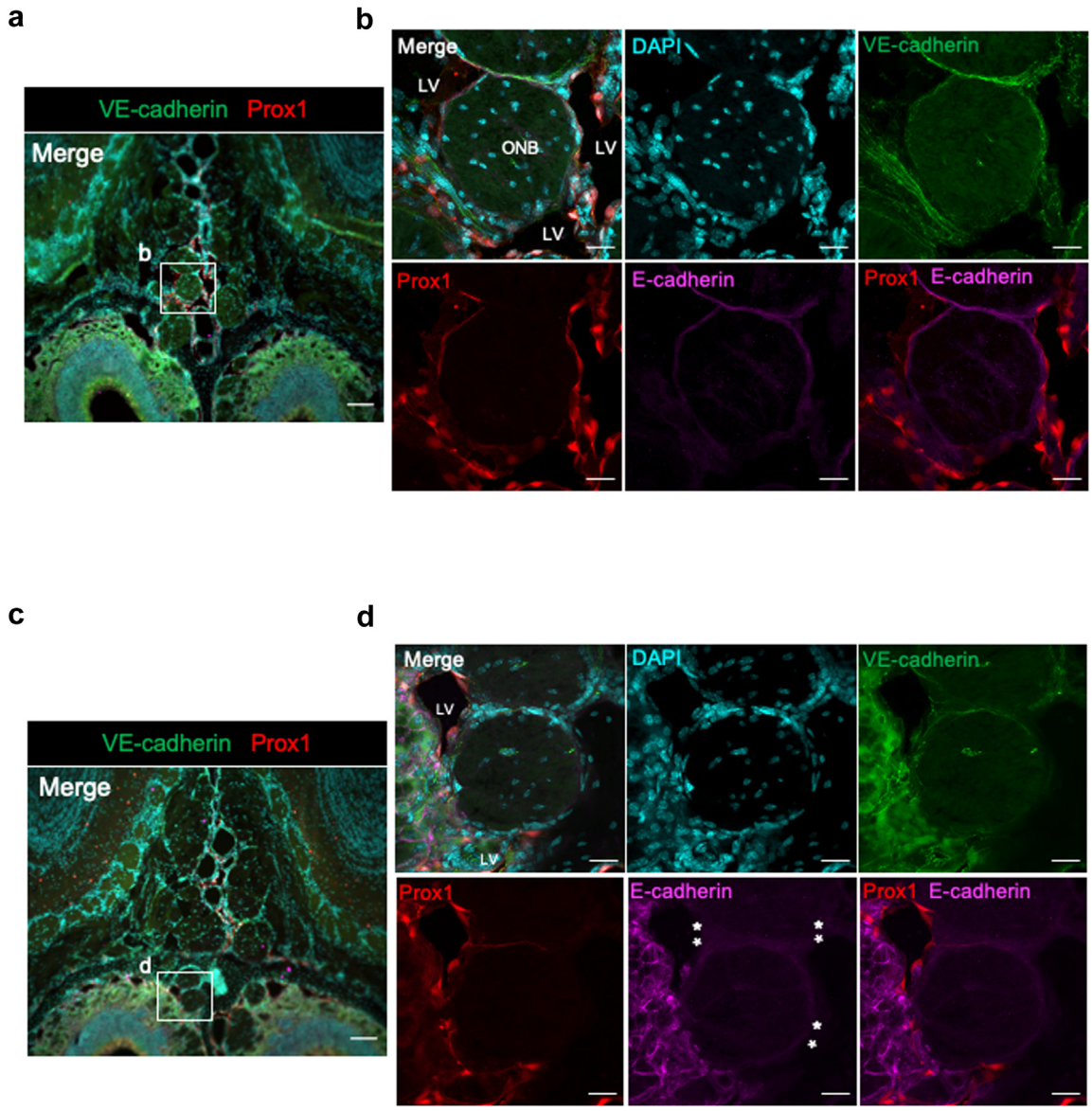

***Fig. 7*: Lack of a defined perineural space around olfactory nerve bundles in mice. a–d**. Representative decalcified images of Prox1-tdTomato x VE-cadherin-GFP transgenic mice immunofluorescently labelled with anti-E-cadherin antibody. **a** and **c**. Pictures were taken with an AxioZoom epifluorescence microscope. Scale bars: 100 µm. **b** and **d**. Magnified confocal pictures of the white insert showing cell nuclei (blue) with DAPI staining. VE-cadherin-GFP signal (green) is visible around the olfactory nerve bundles (ONBs) and in the lymphatic vessels (LVs) (red). Epithelial cells of the arachnoid barrier and in the submucosa were detected with an E-cadherin antibody (magenta). The region on the CNS side of the cribriform plate is depicted in **b**; the nasal submucosa in **d**. Scale bars: 20 µm. Z-stacks were acquired by confocal microscope and were reconstructed with sum intensity projection (SIP) using Fiji software. White asterisks indicate discontinuity of the arachnoid barrier. Images are representative of n = 5 mice.

cribriform plate form a continuous network with the extracranial lymphatics that drains the CSF toward the cervical lymph nodes. Our findings are in line with MRI data recently published in collaboration with our group in which low-rate infusion of Gadospin D showed that a portion of the CSF drained ventrally under the brain through the basal cisterns and exited through the cribriform plate to be collected by lymphatics in the nasopharyngeal region.[38]

Previous studies have shown discontinuity of the arachnoid barrier layer just above the cribriform plate in rodents,[23,52,53] possibly indicating that lymphatics have direct access to the SAS. We observed that the arachnoid barrier, as assessed by E-cadherin antibody staining, is

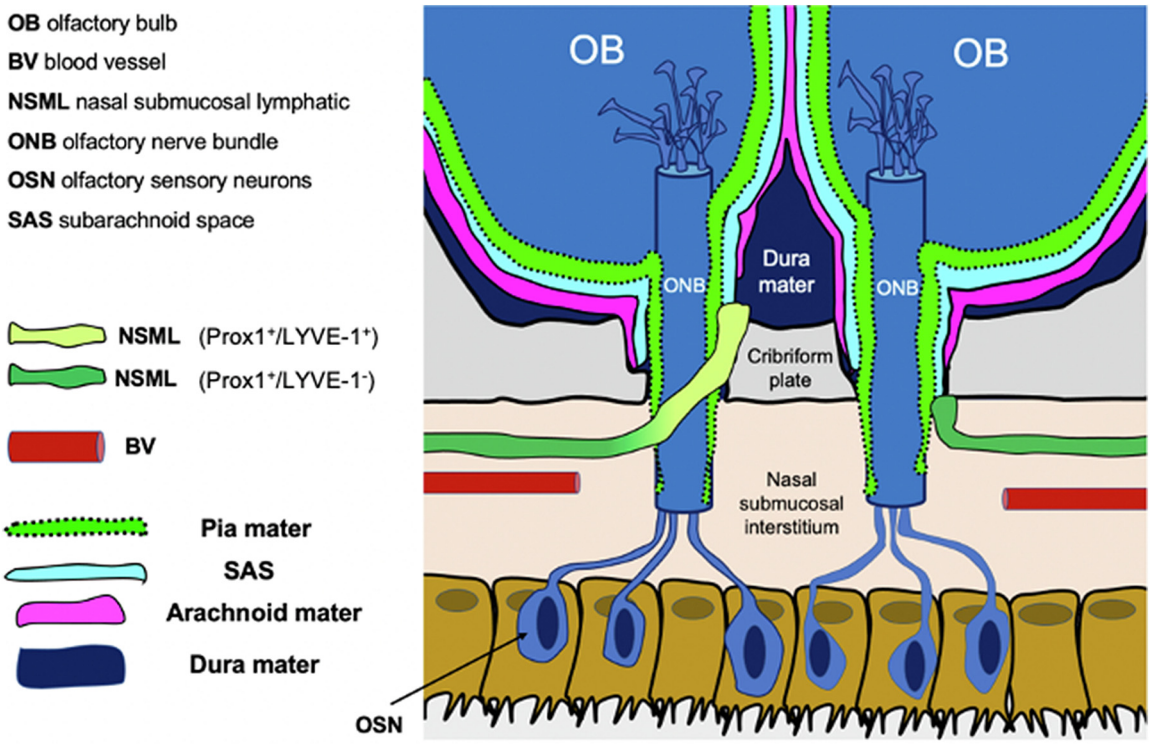

***Fig. 8:* Schematic overview of the drainage pathways alongside olfactory nerve bundles at the mouse cribriform plate region.** The three meningeal layers, pia (green), arachnoid (magenta), and dura mater (dark blue), surround the OBs at the midline and at the ventral aspect of the skull. The olfactory sensory neurons (OSNs) are found at the olfactory epithelium among other cell types (not shown here). The axons of the OSNs converge into ONBs in the lamina propria and cross the cribriform plate via foramina before reaching their terminations in the OB. Blood vessels and lymphatic vessels are embedded in the lamina propria of the nasal submucosa. Here, we show a lymphatic vessel crossing at the midline of the cribriform plate, closely wrapping the ONB (see Figs. 3, 4b and 5b), and reaching the dura mater. CSF drains from the SAS along the ONBs and can enter lymphatic vessels where the arachnoid is interrupted (see Figs. 2 and 3). The pia layer ensheathing the ONB crosses the cribriform plate, and it becomes thinner once it reaches the NSM (see Fig. 7). The arachnoid is discontinuous at the cribriform plate (see Fig. 6c), and it does not seem to be present in the NSM (see Figs. 6d and 7d). Furthermore, we found that LVs crossing the plate and on the CNS side are Prox1^{+}/LYVE-1^{+}, while the ones in the nasal submucosa are Prox1^{+}/LYVE-1^{-} (see Fig. 4), yet form a continuous network of lymphatic vessels draining the CSF towards the cervical lymph nodes (not shown here).

intact on the surface of the OBs, yet becomes discontinuous on the CNS side of the cribriform plate immediately ventral and medial between the OBs, and is completely lacking in the nasal submucosa. This potential discontinuity of the arachnoid barrier further supports our functional data of direct and open communications between the SAS and draining lymphatics in the olfactory region. Recently, work performed within our institute has shown that the adherens junction protein VE-cadherin is a marker for pial and arachnoid leptomeningeal cells in mice (Mapunda et al., submitted). Using a VE-cadherin-GFP reporter mouse, we have shown that VE-cadherin also marks the pia and arachnoid layers around the optic nerve, confirming earlier reports that indicate that the perineural fluid space around the optic nerve (even outside the optic foramen) is a continuation of the SAS.[55] Yet, the anatomical composition of the perineural space around the olfactory nerve bundles has been unclear.[9,62] We found VE-cadherin positive leptomeningeal cells on the surface of the olfactory bulbs and around the olfactory nerve bundles with a stronger expression on the CNS side of the cribriform plate. In the nasal submucosa, VE-cadherin-GFP was weaker and appeared to be confined to a single-cell layer, thus indicating that mice have no defined perineural space in the olfactory region. We hypothesize that this space is compensated for by the presence of LVs that drain the CSF.

This study has potential limitations. We defined open and direct CSF efflux pathways for particles of up to 1 μm size. Further investigations using a broader range of PEGylated beads or labelled cells are needed to understand the nature of the CSF flow in the nasal region. Second, our anatomical characterization of the CSF outflow pathways relies on histology. After the decalcification protocol, we cannot rule out potential

artifacts concerning beads localization due to section processing and tissue preservation. Notably, the nasal route we characterize for the CSF drainage in mice may not have the same relevance in other species due to the different anatomy. Especially in humans, olfactory drainage has been considered a less significant CSF drainage route compared to rodents because of the less pronounced anatomical extension of the nasal cavity. However, a recently published MRI study has shown significant enhancement of intrathecal-administered contrast agent within the nasal turbinates and deep cervical lymph nodes of humans, indicating that similar peri-olfactory nerve pathways for CSF outflow may also exist in our species.[63]

Understanding the CSF clearance pathways to the lymphatic system has immediate relevance for neuroimmunology, as the pathways for antigens and immune cells from the CNS to the lymph nodes have not yet been completely elucidated. Furthermore, it would improve our understanding of the possible mechanism of the clearance of soluble proteins such as amyloid-beta and tau in neurodegenerative disorders, as well as erythrocytes and their breakdown products after intracranial haemorrhagic stroke. Finally, improved knowledge of the anatomical routes across the cribriform plate will help optimize drug delivery via intranasal administration to the CNS.[64]

Contributors

I.S., N.C., M.R., and S.T.P. conceived and designed the study; I.S., N.C., M.R., and S.T.P. performed in vivo experiments and imaging; I.S., N.C., and A.C., performed the histology and processed the data; A.K., S.A., and P.L. developed and provided the PEGylated fluorescent beads and the near-infrared P40D800 tracer; J.A.M. and B.E. provided the Prox1-tdTomato x VE-cadherin transgenic mice for the study; I.S., N.C., and S.T.P. drafted the manuscript. M.D., B.E., and M.V. critically discussed the results of the study. I.S. and S.T.P. have verified the underlying data and have the final responsibility for the decision to submit for publication. All the authors have read and approved the final version of the manuscript.

Data sharing statement

All underlying data of this study will be made available from the corresponding author upon reasonable request.

Declaration of interests

The authors declare no conflict of interests.

Acknowledgments

This study was supported by the Swiss National Science Foundation (310030_189226), Dementia Research Switzerland—Synapsis Foundation, the Heidi Seiler Stiftung and the Fondation Dr. Corinne Schuler. We would like to thank Elisa Bouillet for sharing her expertise in animal surgery and Jeannette Scholl for her excellent technical assistance. We thank Urban Deutsch for assisting the transgenic mice generation. We acknowledge the Microscopy Imaging Center, University of Bern, Switzerland, for microscopy equipment support.

Appendix A. Supplementary data

Supplementary data related to this article can be found at https://doi.org/10.1016/j.ebiom.2023.104558.

References

1 Louveau A, Plog BA, Antila S, Alitalo K, Nedergaard M, Kipnis J. Understanding the functions and relationships of the glymphatic system and meningeal lymphatics. *J Clin Invest*. 2017;127(9):3210–3219.
2 Proulx ST. Cerebrospinal fluid outflow: a review of the historical and contemporary evidence for arachnoid villi, perineural routes, and dural lymphatics. *Cell Mol Life Sci*. 2021;78(6):2429–2457.
3 Davson H, Segal MB. *Physiology of the CSF and blood-brain barriers*. Boca Raton etc.: CRC Press; 1996:822.
4 Key A, Retzius G. *Studien in der Anatomie des Nervensystems und des Bindegewebes*. Stockholm; Stockholm: Samson & Wallin; 1875:220.
5 Weed LH. Studies on cerebro-spinal fluid. No. III: the pathways of escape from the subarachnoid spaces with particular reference to the arachnoid villi. *J Med Res*. 1914;31(1):51–91.
6 Shah T, Leurgans SE, Mehta RI, et al. Arachnoid granulations are lymphatic conduits that communicate with bone marrow and dura-arachnoid stroma. *J Exp Med*. 2023;220(2):e20220618.
7 Bradbury MWB, Cserr HF. Drainage of cerebral interstitial fluid and of cerebrospinal fluid into lymphatics. In: Johnston MG, ed. *Experimental biology of the lymphatic circulation*. Amsterdam: Elsevier; 1985:355–394.
8 McComb JG. Recent research into the nature of cerebrospinal fluid formation and absorption. *J Neurosurg*. 1983;59(3):369–383.
9 Koh L, Zakharov A, Johnston M. Integration of the subarachnoid space and lymphatics: is it time to embrace a new concept of cerebrospinal fluid absorption? *Cerebrospinal Fluid Res*. 2005;2:6.
10 Pollay M. The function and structure of the cerebrospinal fluid outflow system. *Cerebrospinal Fluid Res*. 2010;7:9.
11 Ma Q, Ineichen BV, Detmar M, Proulx ST. Outflow of cerebrospinal fluid is predominantly through lymphatic vessels and is reduced in aged mice. *Nat Commun*. 2017;8(1):1434.
12 Ma Q, Ries M, Decker Y, et al. Rapid lymphatic efflux limits cerebrospinal fluid flow to the brain. *Acta Neuropathol*. 2019;137(1):151–165.
13 Ma Q, Decker Y, Müller A, Ineichen BV, Proulx ST. Clearance of cerebrospinal fluid from the sacral spine through lymphatic vessels. *J Exp Med*. 2019;216(11):2492–2502.
14 Hutchings M, Weller RO. Anatomical relationships of the pia mater to cerebral blood vessels in man. *J Nurosurg*. 1986;65(3):316–325.
15 Zhang ET, Inman CB, Weller RO. Interrelationships of the pia mater and the perivascular (Virchow-Robin) spaces in the human cerebrum. *J Anat*. 1990;170:111–123.
16 DeSisto J, O'Rourke R, Jones HE, et al. Single-cell transcriptomic analyses of the developing meninges reveal meningeal fibroblast diversity and function. *Dev Cell*. 2020;54(1):43–59.e4.
17 Alcolado R, Weller RO, Parrish EP, Garrod D. The cranial arachnoid and pia mater in man: anatomical and ultrastructural observations. *Neuropathol Appl Neurobiol*. 1988;14(1):1–17.
18 Nabeshima S, Reese TS, Landis DM, Brightman MW. Junctions in the meninges and marginal glia. *J Comp Neurol*. 1975;164(2):127–169.
19 Yasuda K, Cline C, Vogel P, et al. Drug transporters on arachnoid barrier cells contribute to the blood-cerebrospinal fluid barrier. *Drug Metab Dispos*. 2013;41(4):923–931.
20 Holman DW, Grzybowski DM, Mehta BC, Katz SE, Lubow M. Characterization of cytoskeletal and junctional proteins expressed by cells cultured from human arachnoid granulation tissue. *Cerebrospinal Fluid Res*. 2005;2:9.
21 Balin BJ, Broadwell RD, Salcman M, el-Kalliny M. Avenues for entry of peripherally administered protein to the central nervous system in mouse, rat, and squirrel monkey. *J Comp Neurol*. 1986;251(2):260–280.
22 Brøchner CB, Holst CB, Møllgård K. Outer brain barriers in rat and human development. *Front Neurosci*. 2015;9:1–16.
23 Hsu M, Laaker C, Madrid A, et al. Neuroinflammation creates an immune regulatory niche at the meningeal lymphatic vasculature near the cribriform plate. *Nat Immunol*. 2022;23(4):581–593.
24 Coles JA, Myburgh E, Brewer JM, McMenamin PG. Where are we? The anatomy of the murine cortical meninges revisited for intravital imaging, immunology, and clearance of waste from the brain. *Prog Neurobiol*. 2017;156:107–148.
25 Proulx ST, Engelhardt B. Central nervous system zoning: how brain barriers establish subdivisions for CNS immune privilege and immune surveillance. *J Intern Med*. 2022;292(1):47–67.

26 Aspelund A, Antila S, Proulx ST, et al. A dural lymphatic vascular system that drains brain interstitial fluid and macromolecules. *J Exp Med*. 2015;212(7):991–999.
27 Louveau A, Smirnov I, Keyes TJ, et al. Structural and functional features of central nervous system lymphatic vessels. *Nature*. 2015;523(7560):337–341.
28 Ahn JH, Cho H, Kim JH, et al. Meningeal lymphatic vessels at the skull base drain cerebrospinal fluid. *Nature*. 2019;572:62–66.
29 Jacob L, Boisserand LSB, Geraldo LHM, et al. Anatomy and function of the vertebral column lymphatic network in mice. *Nat Commun*. 2019;10:1–16.
30 Pizzo ME, Wolak DJ, Kumar NN, et al. Intrathecal antibody distribution in the rat brain: surface diffusion, perivascular transport and osmotic enhancement of delivery. *J Physiol*. 2018;596(3):445–475.
31 Brady M, Rahman A, Combs A, et al. Cerebrospinal fluid drainage kinetics across the cribriform plate are reduced with aging. *Fluids Barriers CNS*. 2020;17(1):71.
32 Stanton EH, Persson NDA, Gomolka RS, et al. Mapping of CSF transport using high spatiotemporal resolution dynamic contrast-enhanced MRI in mice: effect of anesthesia. *Magn Reson Med*. 2021;85(6):3326–3342.
33 Kwon S, Janssen CF, Velasquez FC, Sevick-Muraca EM. Fluorescence imaging of lymphatic outflow of cerebrospinal fluid in mice. *J Immunol Methods*. 2017;449:37–43.
34 Bradbury MW, Westrop RJ. Factors influencing exit of substances from cerebrospinal fluid into deep cervical lymph of the rabbit. *J Physiol*. 1983;339:519–534.
35 Erlich SS, McComb JG, Hyman S, Weiss MH. Ultrastructural morphology of the olfactory pathway for cerebrospinal fluid drainage in the rabbit. *J Neurosurg*. 1986;64(3):466–473.
36 Kida S, Pantazis A, Weller RO. CSF drains directly from the subarachnoid space into nasal lymphatics in the rat. Anatomy, histology and immunological significance. *Neuropathol Appl Neurobiol*. 1993;19(6):480–488.
37 Norwood JN, Zhang Q, Card D, Craine A, Ryan TM, Drew PJ. Anatomical basis and physiological role of cerebrospinal fluid transport through the murine cribriform plate. *Elife*. 2019;8:1–32.
38 Decker Y, Kramer J, Xin L, et al. Magnetic resonance imaging of cerebrospinal fluid outflow after low-rate lateral ventricle infusion in mice. *JCI Insight*. 2022;7(3):e150881.
39 Yoffey JM, Drinker CK. Some observations on the lymphatics of the nasal mucous membrane in the cat and monkey. *J Anat*. 1939;74(Pt 1):45–52.3.
40 Antila S, Karaman S, Nurmi H, et al. Development and plasticity of meningeal lymphatic vessels. *J Exp Med*. 2017;214(12):3645–3667.
41 Hsu M, Rayasam A, Kijak JA, et al. Neuroinflammation-induced lymphangiogenesis near the cribriform plate contributes to drainage of CNS-derived antigens and immune cells. *Nat Commun*. 2019;10:229.
42 Louveau A, Herz J, Alme MN, et al. CNS lymphatic drainage and neuroinflammation are regulated by meningeal lymphatic vasculature. *Nat Neurosci*. 2018;21(10):1380–1391.
43 Hsu M, Sandor M, Fabry Z. Current concepts on communication between the central nervous system and peripheral immunity via lymphatics: what roles do lymphatics play in brain and spinal cord disease pathogenesis? *Biol Futur*. 2021;72(1):45–60.
44 Jacob L, de Brito Neto J, Lenck S, et al. Conserved meningeal lymphatic drainage circuits in mice and humans. *J Exp Med*. 2022;219(8):e20220035.
45 Choi I, Chung HK, Ramu S, et al. Visualization of lymphatic vessels by Prox1-promoter directed GFP reporter in a bacterial artificial chromosome-based transgenic mouse. *Blood*. 2011;117(1):362–365.
46 Proulx ST, Luciani P, Christiansen A, et al. Use of a PEG-conjugated bright near-infrared dye for functional imaging of rerouting of tumor lymphatic drainage after sentinel lymph node metastasis. *Biomaterials*. 2013;34(21):5128–5137.
47 Polomska AK, Proulx ST. Imaging technology of the lymphatic system. *Adv Drug Deliv Rev*. 2021;170:294–311.
48 Faber WM. The nasal mucosa and the subarachnoid space. *Am J Anat*. 1937;62(1):121–148.
49 Field EJ, Brierley JB. The lymphatic connexions of the subarachnoid space; an experimental study of the dispersion of particulate matter in the cerebrospinal fluid, with special reference to the pathogenesis of poliomyelitis. *Br Med J*. 1948;1(4563):1167–1171.
50 Gomez DG, Fenstermacher JD, Manzo RP, Johnson D, Potts DG. Cerebrospinal fluid absorption in the rabbit: olfactory pathways. *Acta Otolaryngol*. 1985;100(5–6):429–436.
51 Harkema JR, Carey SA, Wagner JG. The nose revisited: a brief review of the comparative structure, function, and toxicologic pathology of the nasal epithelium. *Toxicol Pathol*. 2006;34(3):252–269.
52 Weller RO, Sharp MM, Christodoulides M, Carare RO, Møllgård K. The meninges as barriers and facilitators for the movement of fluid, cells and pathogens related to the rodent and human CNS. *Acta Neuropathol*. 2018;135:363–385.
53 Walter BA, Valera VA, Takahashi S, Ushiki T. The olfactory route for cerebrospinal fluid drainage into the peripheral lymphatic system. *Neuropathol Appl Neurobiol*. 2006;32:388–396.
54 Derk J, Como CN, Jones HE, et al. Formation and function of the meningeal arachnoid barrier around the developing mouse brain. *Dev Cell*. 2023;58:1–10. https://doi.org/10.1016/j.devcel.2023.03.005.
55 Shen JY, Kelly DE, Hyman S, McComb JG. Intraorbital cerebrospinal fluid outflow and the posterior uveal compartment of the hamster eye. *Cell Tissue Res*. 1985;240(1):77–87.
56 Greenwald RB, Choe YH, McGuire J, Conover CD. Effective drug delivery by PEGylated drug conjugates. *Adv Drug Deliv Rev*. 2003;55(2):217–250.
57 Johnston M, Zakharov A, Papaiconomou C, Salmasi G, Armstrong D. Evidence of connections between cerebrospinal fluid and nasal lymphatic vessels in humans, non-human primates and other mammalian species. *Cerebrospinal Fluid Res*. 2004;1(1):2.
58 Zakharov A, Papaiconomou C, Johnston M. Lymphatic vessels gain access to cerebrospinal fluid through unique association with olfactory nerves. *Lymphat Res Biol*. 2004;2(3):139–146.
59 Furukawa M, Shimoda H, Kajiwara T, Kato S, Yanagisawa S. Topographic study on nerve-associated lymphatic vessels in the murine craniofacial region by immunohistochemistry and electron microscopy. *Biomed Res*. 2008;29(6):289–296.
60 Ulvmar MH, Makinen T. Heterogeneity in the lymphatic vascular system and its origin. *Cardiovasc Res*. 2016;111(4):310–321.
61 Petrova TV, Koh GY. Biological functions of lymphatic vessels. *Science*. 2020;369(6500):eaax4063.
62 Jackson RT, Tigges J, Arnold W. Subarachnoid space of the CNS, nasal mucosa, and lymphatic system. *Arch Otolaryngol*. 1979;105(4):180–184.
63 Zhou Y, Ran W, Luo Z, et al. Impaired peri-olfactory cerebrospinal fluid clearance is associated with ageing, cognitive decline and dyssomnia. *eBioMedicine*. 2022;86:104381.
64 Lochhead JJ, Thorne RG. Intranasal delivery of biologics to the central nervous system. *Adv Drug Deliv Rev*. 2012;64(7):614–628.